CHAPTER 3

FOLDABLE CYLINDRICAL TUBE AS NEW STENT GRAFT

A stent graft is a tubular foldable structure as discussed in Chapter 1. In this chapter, a new type of an innovative stent graft is developed based on novel folding patterns of the cylindrical tube. The chapter deals mainly with the geometric aspects of the stent graft.

A new design of the foldable cylindrical tube is considered in Sections 3.1 in which the tube is divided into a number of foldable elements. Section 3.2 gives the geometric properties of a basic element such as radius. Condition regarding the connection of the basic elements in a longitudinal direction is considered in Section 3.3. In the following sections, Sections 3.4 and 3.5, other geometric properties of the foldable cylindrical tube such as length and deformation are defined and analysed. Section 3.6 generalises the basic element and its geometric properties are also defined. In Section 3.7, the results of the geometric properties of the new stent graft are discussed. This is followed by a discussion of variations of the folding patterns in Section 3.8 for both cylindrical and conical tubes. Section 3.9 concludes this chapter.

It is important to note that the analysis presented in this chapter is purely geometric in which material deformation during deployment and the thickness of the models are not considered.

3.1 Foldable cylindrical tube as a stent graft

The crucial requirement in the design of a cylindrical tubular stent graft is that it can be folded in its radial direction, and when folded its radius is minimised so that it can be delivered to the human body with ease. To achieve compact packaging of the tubular stent graft, carefully designed folds are introduced. These folds will behave as line hinges so that more complex joints or sliding wires are not required. The stent graft must also have a simple structural form. The pattern of the folds used in the stent graft is inspired by the *pineapple folding pattern* using triangular units (Kresling 1995).

Figure 3.1 shows photographs of the foldable cylindrical tube model with a pineapple folding pattern made of a single sheet of paper in its fully folded and deployed configurations, respectively. It becomes a cylindrical tube in the fully expanded configuration.

The details of the folding pattern are given in Figure 3.2. The solid and broken lines represent hill and valley folds which form peak and trough creases, respectively. As shown in Figure 3.2(a), the element has a square shape and its folding pattern is symmetrical both vertically and horizontally. As shown in Figure 3.2(b), the pattern of the folds comprises the square elements which are repeated over the entire area of the sheet. The total numbers of the elements in horizontal and vertical directions are denoted as m and n, respectively. The elements on even rows are shifted half an element in comparison with those on odd rows illustrated in bold outline in the figure. The opposite edges of the sheet, a_1-a_2-a_3 and b_1-b_2-b_3 are joined together to form a cylindrical tube. It is also noted from Figure 3.2(b) that there are six folds intersecting at those points marked by black dots. They satisfy Equations (2.4) and (2.5) which are the fundamental relations of the number of the hill and valley folds and of the angles for folding a sheet as described in Chapter 2.

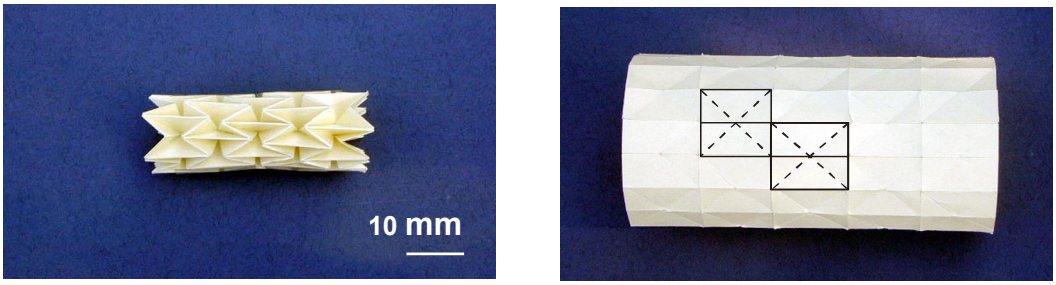

Figure 3.1 Photographs of the foldable cylindrical tube with a pineapple folding pattern in its (a) fully folded and (b) fully deployed configurations.

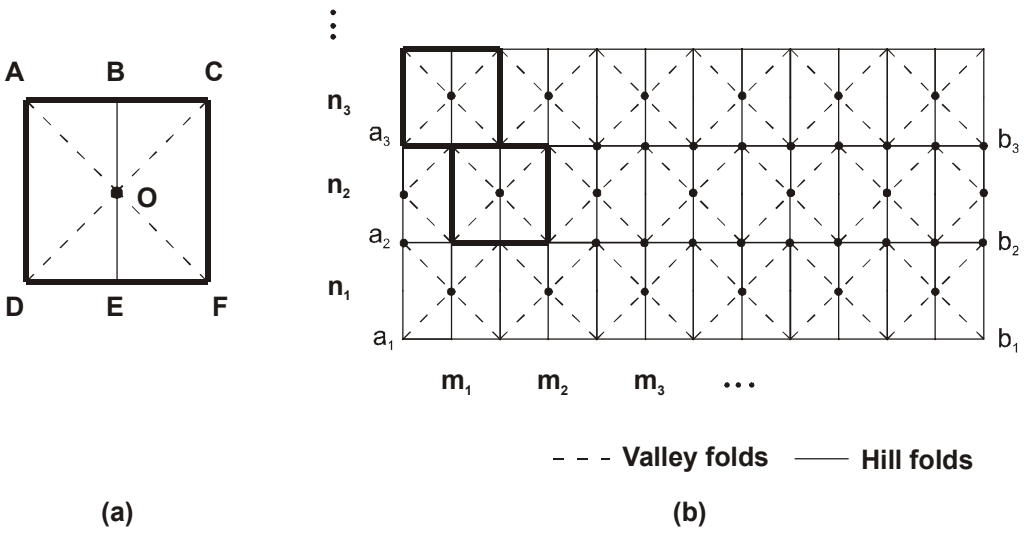

Figure 3.2 (a) A basic element and (b) development of the basic pattern.

One of the most interesting properties of the folding pattern is that it causes the cylinder to fold and expand both longitudinally and radially. Hence, both the length and the diameter of the tube decrease during folding and increase during expanding. The folded configuration of each element also makes the tube flexible. These properties are suitable for the stent graft design because it can be packaged compactly and it has a

certain amount of flexibility when folded. Furthermore, the folds rather than a more complex hinging mechanism allow the stent graft to fold neatly and expand simply without causing any such problems as tangling and rupturing.

3.2 Generalised rectangular element

3.2.1 The element

The pineapple folding pattern is, in fact, a special case of a family of more general folding patterns. Consider a more general rectangular basic element shown in Figure 3.3(a). The angles $\angle DAO$ and $\angle OAB$ can be denoted as α_1 and α_2, respectively, and $\alpha_1 + \alpha_2 = 90^o$. Let l represent the length AB ($AB = AC/2$). Obviously, a row of such elements can be mapped onto a sheet, see Figure 3.3(b). By joining a_1-a_2 with b_1-b_2, a tube is formed.

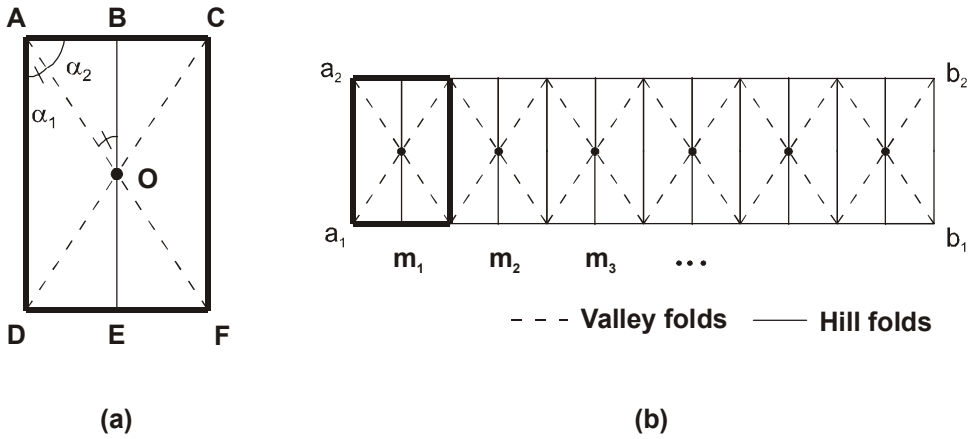

Figure 3.3 (a) Generalised rectangular element and (b) formation of a tube with such elements.

3.2.2 Central and deployment angles

Figure 3.4 shows a perspective view of the foldable cylindrical tube formed by a single row of the rectangular elements. The *central angle*, δ, is defined as $\angle AO_0C/2$, which depends on the number of the circumferential elements, *m*, and can be calculated as

$$\delta = \frac{360^o}{2m} = \frac{180^o}{m} \tag{3.1}$$

δ must remain constant during deployment.

Now consider a single element of the tube during deployment, shown by the perspective view in Figures 3.5(a)-(c). It is assumed that the rest of the elements behave exactly the same. It should be pointed out that the deployment of the tube goes through two phases. During the first phase, the element deploys until nodes A, B and C become co-liner, i.e., the rectangular element is flattened. The *deployment angle*, θ, is defined as $\angle ABC/2$. When the tube is fully folded, node O will reach the projection position of O_0, and θ becomes the fully folded deployment angle, θ_0. From Figure 3.5(a),

$$AQ = AB\sin\theta_0 = l\sin\theta_0 \tag{3.2}$$

and from Figure 3.5(d),

$$AQ = O_0A\sin\delta \tag{3.3}$$

When O and the projection of O_0 overlap, $O_0A = OA\sin\alpha_1 = l$,

$$\theta_0 = \delta \tag{3.4}$$

During the first phase θ alters from θ_0 to 90^o.

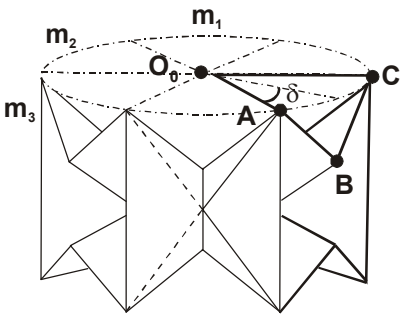

Figure 3.4 Perspective view of a tube formed by a row of the rectangular elements.

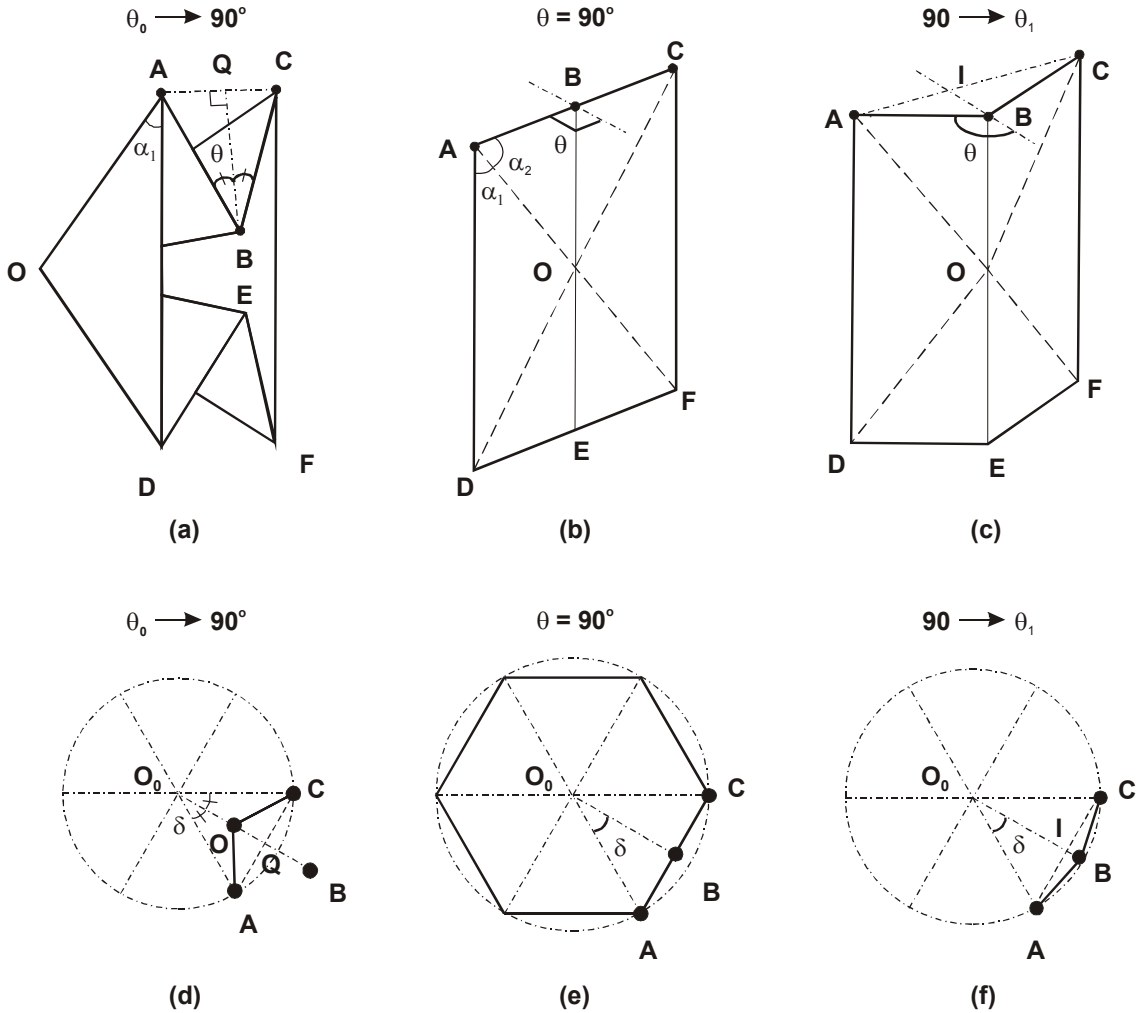

Figure 3.5 (a), (b) and(c) Perspective and (d), (e) and (f) projective views of a single element during deployment.

Then, on the second phase of deployment the central crease between nodes B and E moves outwards in the radial direction. In order to make θ larger than 90^o and continually increase as the tube deploys, the *deployment angle*, θ, is redefined as an outside angle (angle more than 90^o and less than 180^o) as shown in Figure 3.5(c). θ reaches θ_1, the fully expanded deployment angle, when the tube is fully deployed. For this instance,

$$\theta_1 = 180^o - \angle ABO_0 \tag{3.5}$$

where

$$\angle ABO_0 = \frac{180^o - \delta}{2} \tag{3.6}$$

Thus

$$\theta_1 = 90^o + \frac{\delta}{2} \tag{3.7}$$

Table 3.1 shows how the deployable angles, θ_0 and θ_1, in its fully folded and expanded forms, vary with the different values of the number of elements, *m*. As *m* increases, both θ_0 and θ_1 decrease.

Table 3.1 Deployment angles vs. *m*

m	4	6	8	9	12	18
θ_0 (deg.)	45	30	22.5	20	15	10
θ_1 (deg.)	112.5	105	101.25	100	97.5	95

3.2.3 Radius during deployment

The radius of the stent graft is one of the most important geometric properties measured during the deployment process of the cylindrical tube. It is possible to calculate the change in radius during deployment of the foldable cylindrical tube using a single row of the rectangle elements.

Based on the projection of the tube, see Figure 3.5(a), denote

$$R_{o1} = O_0 B \tag{3.8}$$

$$R_{o2} = O_0 A \tag{3.9}$$

and

$$R_i = O_0 O \tag{3.10}$$

where O_0 is a node at a central axis in a longitudinal direction.

During the first phase of deployment, i.e., $\theta_0 \le \theta \le 90^o$, a typical element is shown in Figure 3.6. Combining it with Figure 3.5(d) gives

$$R_{o1} = O_0 B = \frac{AC/2}{\tan\delta} + O'B \tag{3.11}$$

$$R_{o2} = O_0 A = \frac{AC/2}{\sin\delta} \tag{3.12}$$

$$R_i = O_0 O = \frac{AC/2}{\tan\delta} - OO'_p \tag{3.13}$$

where

$$AC = 2l\sin\theta \tag{3.14}$$

Substituting Equation (3.14) into (3.12) gives

$$R_{o2} = \frac{l\sin\theta}{\sin\delta} \tag{3.15}$$

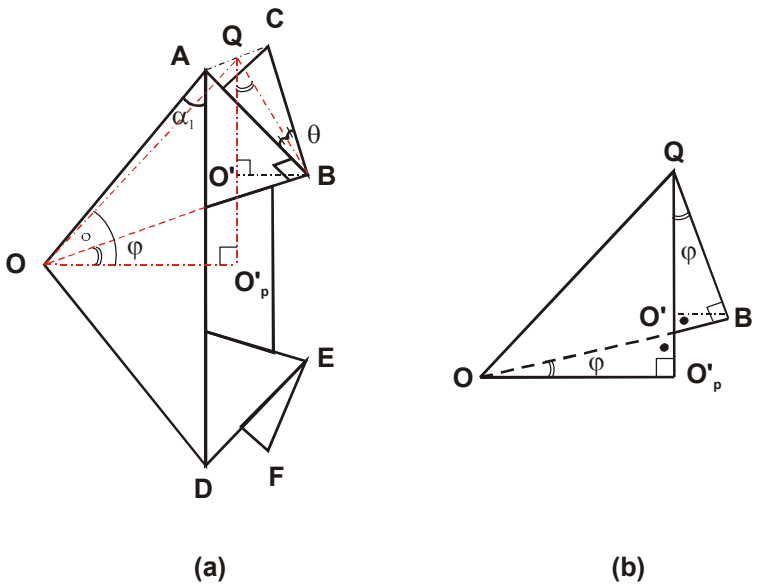

Figure 3.6 Rectangular element during the first phase of deployment. (a) Perspective view and (b) side projection of the top half of the element.

It is noted that in Figure 3.6(a) node B sticks out off the plane formed by nodes A, C, F and D by length *O'B*. Because *OB* is perpendicular to both *AB* and *BC*, *OB* is also perpendicular to *BQ*. From Figure 3.6(b), *O'B* is given by

$$O'B = BQ\sin\varphi = l\cos\theta\sin\varphi \tag{3.16}$$

where

$$\varphi = \angle BQO' = \angle O'OO'_{\mathrm{p}} = \angle QOO'_{\mathrm{p}} - \angle QOB \tag{3.17}$$

Back to Figure 3.6(a) again,

$$\angle QOO'_{\mathrm{p}} = \arcsin\left(\frac{QO'_{\mathrm{p}}}{OQ}\right) = \arcsin\left(\frac{AD}{2OQ}\right) \tag{3.18}$$

and

$$\angle QOB = \arccos\left(\frac{OB}{OQ}\right) \tag{3.19}$$

while

$$AD = \frac{2l}{\tan\alpha_1},\ OB = \frac{AD}{2} = \frac{l}{\tan\alpha_1} \tag{3.20}$$

and

$$OQ = \sqrt{OA^2 - AQ^2} \tag{3.21}$$

where

$$OA = \frac{l}{\sin\alpha_1},\ AQ = l\sin\theta \tag{3.22}$$

Substituting Equations (3.20) to (3.22) into (3.18) and (3.19) and then into (3.17) gives

$$\varphi = \arcsin\left(\frac{AD}{2OQ}\right) - \arccos\left(\frac{OB}{OQ}\right)$$

$$= \arcsin\left(\frac{\cos\alpha_1}{\sqrt{1-\sin^2\theta\sin^2\alpha_1}}\right) - \arccos\left(\frac{\cos\alpha_1}{\sqrt{1-\sin^2\theta\sin^2\alpha_1}}\right) \tag{3.23}$$

Hence, from Equation (3.16)

$$O'B = l\cos\theta\sin\left[\arcsin\left(\frac{\cos\alpha_1}{\sqrt{1-\sin^2\theta\sin^2\alpha_1}}\right) - \arccos\left(\frac{\cos\alpha_1}{\sqrt{1-\sin^2\theta\sin^2\alpha_1}}\right)\right]$$

$$= l\cos\theta\frac{\cos^2\alpha_1 - \sin^2\alpha_1\cos^2\theta}{1-\sin^2\theta\sin^2\alpha_1} \tag{3.24}$$

Thus, using Equation (3.11)

$$R_{o1}=\frac{l\sin\theta}{\tan\delta}+l\cos\theta\frac{\cos^2\alpha_1-\sin^2\alpha_1\cos^2\theta}{1-\sin^2\theta\sin^2\alpha_1} \tag{3.25}$$

For the basic rectangle element, as shown in Figure 3.6, $OB=QO'_p$. $\Delta OQO'_p$ and ΔOQB are therefore equal triangles, so,

$$OO'_p=QB=l\cos\theta \tag{3.26}$$

Substituting Equation (3.26) into (3.13) gives

$$R_i=\frac{l\sin\theta}{\tan\delta}-l\cos\theta \tag{3.27}$$

On the second phase of deployment, i.e., θ varies from 90^o to θ_1, see Figures 3.5(c) and (f). With regards to the radii, it is found that

$$R_{o1}=\frac{AC/2}{\tan\delta}+IB=\frac{l\sin\theta}{\tan\delta}-l\cos\theta \tag{3.28}$$

$$R_{o2}=\frac{AC/2}{\sin\delta}=\frac{l\sin\theta}{\sin\delta} \tag{3.29}$$

$$R_i=R_{o1}=\frac{l\sin\theta}{\tan\delta}-l\cos\theta \tag{3.30}$$

in which

$$IB=-l\cos\theta \tag{3.31}$$

Then, when the tube is fully deployed, i.e., $\theta = \theta_1$,

$$R_i = R_{o1} = R_{o2} = \frac{l}{2\sin\frac{\delta}{2}} \tag{3.32}$$

Results of the radii with various α_1 and m during deployment will be given in Section 3.7.

3.3 Connection of the elements in a longitudinal direction

In the previous section only a single row of the elements has been considered. However, elements are also connected in a longitudinal direction to form a long foldable cylindrical tube as shown in Figure 3.2(b) where a row of the elements are shifted by a half element with respect to the neighbouring rows. Let us draw attention to the rectangle elements which are located on two adjacent rows and they are to be connected together, see Figure 3.7. Now we will try to identify the condition in order to design the foldable cylindrical tube with the rectangle elements. The key values of the element angle α_1 and element number m will be discussed.

In Figure 3.7, before the top element is connected to the lower element the radii of nodes E_2 and F_2 are R_{o1} and R_{o2}, respectively, which have been defined in the previous section. For the lower element, assuming that it behaves exactly the same as the upper element during deployment, the radii of nodes A_1 and B_1 are R_{o2} and R_{o1}, respectively, before it is connected to the element above. To enable these two rows of the elements to be connected with full geometric compatibility, the radii of nodes E_2 and A_1, and nodes F_2 and B_1 must be equal throughout the deployment, i.e.,

$$R_{o1} = R_{o2} \tag{3.33}$$

or

$$\frac{l\sin\theta}{\tan\delta}+l\cos\theta\frac{\cos^2\alpha_1-\sin^2\alpha_1\cos^2\theta}{1-\sin^2\theta\sin^2\alpha_1}=\frac{l\sin\theta}{\sin\delta} \tag{3.34}$$

on the first phase of deployment from Equations (3.25) and (3.15), and,

$$\frac{l\sin\theta}{\tan\delta}-l\cos\theta=\frac{l\sin\theta}{\sin\delta} \tag{3.35}$$

on the second phase of deployment from Equations (3.28) and (3.29).

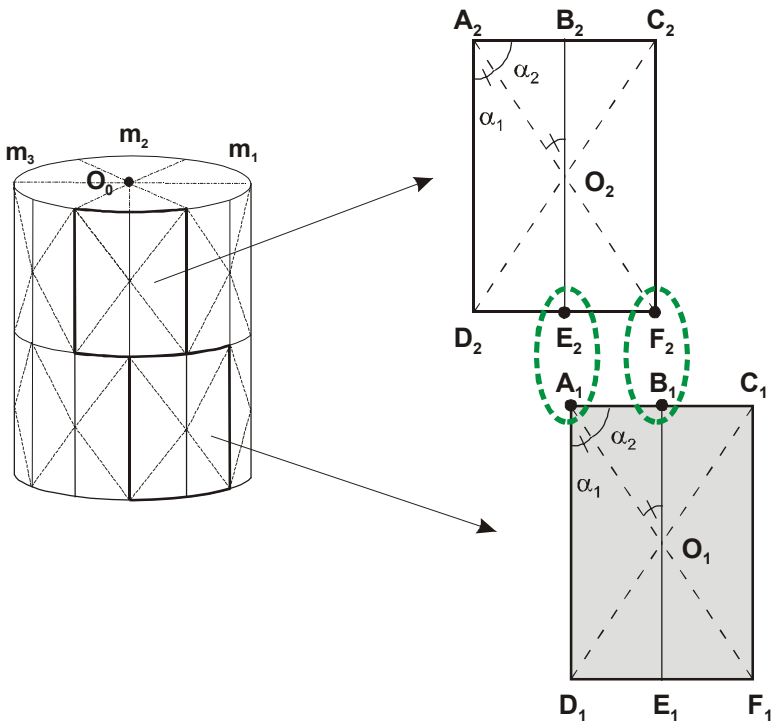

Figure 3.7 Connection of two adjacent elements.

However, it has been found that Equations (3.34) and (3.35) hold only for certain deployable angles θ's . For instance, when $m = 6$, Equation (3.1) gives $\delta = 180^{\circ} / 6 = 30^{\circ}$ and if $\alpha_1 = 45^{\circ}$, Equation (3.34) holds if $\theta = 33^{\circ}$ and $\theta = 72^{\circ}$, and Equation (3.35) holds for $\theta = 105^{\circ}$ where the tube is fully deployed at the end of phase two. Hence mismatch between R_{o1} and R_{o2} is occurring during deployment so that the tube deforms during deployment. The value of the difference between R_{o1} and R_{o2}, normalised by the length of nodes A and B, l, is denoted as y, which is

$$y = \frac{R_{o1} - R_{o2}}{l} \tag{3.36}$$

The optimum design which can be minimised the deformation of the tube is that where y is close to zero.

For m = 6, Figure 3.8 shows curves of y against θ for various α_1 and α_2 where $\alpha_1 + \alpha_2 = 90^{\circ}$. When $\alpha_1 = 45^{\circ}$, the value of y becomes zero when $\theta = 33^{\circ}, 72^{\circ}$ and 105° as indicated earlier. Also, when $\alpha_1 = 30^{\circ}$, the value of y becomes zero when $\theta = 74^{\circ}$ and 105°. When $\alpha_1 = 60^{\circ}$, the value of y becomes zero only when $\theta = 105^{\circ}$, i.e., the tube is fully folded. It is obvious that the value of y is closer to zero for every θ when $\alpha_1 = 45^{\circ}$ than when $\alpha_1 = 30^{\circ}$ or 60°. Therefore, the optimal angle α_1 could be approximately 45°. In the following, we will try to define and calculate a precise value of the optimal value of α_1.

A value M of $|y|$ during deployment is considered, which is given by

$$M = \int_{\theta_0}^{\theta_1} |y| \, \mathrm{d}\theta \tag{3.37}$$

where $\int_{\theta_0}^{\theta_1} |y| \, \mathrm{d}\theta$ is the area bounded by the curve y and the axis of $y = 0$ in Figure 3.8, and the ordinates at θ_0 and θ_1 which are deployment angles when the tube is fully

folded and expanded. M becomes minimal with respect to α_1 under the following condition

$$\frac{\mathrm{d}M}{\mathrm{d}\alpha_1} = 0 \tag{3.38}$$

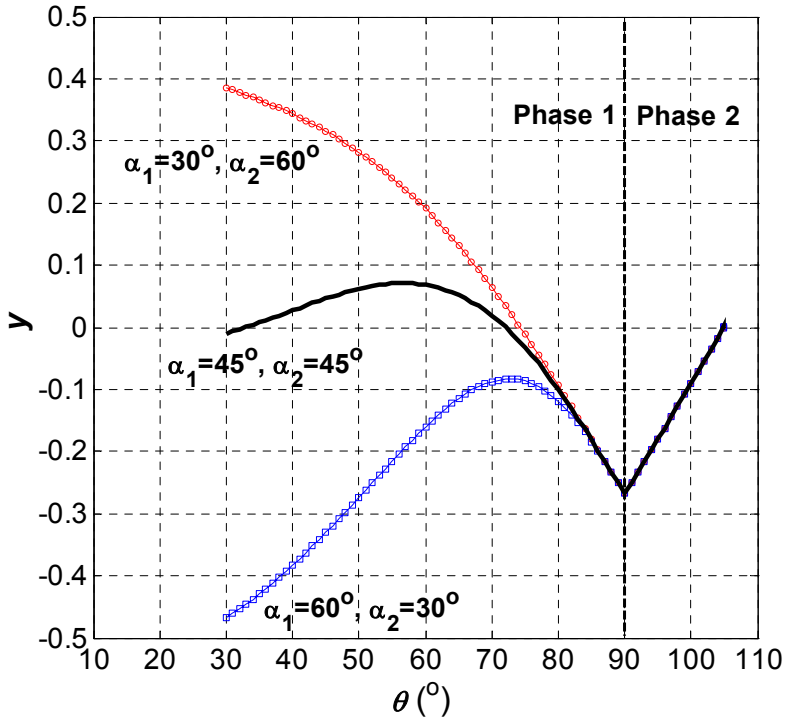

Figure 3.8 y vs. θ for the rectangle elements with various α_1 when m = 6.

From Equation (3.38), it is found that for m = 6 M becomes minimum when $\alpha_1 = 46.7^{\circ}$. The value of y with respect to θ for the rectangle elements when $\alpha_1 = 45^{\circ}$ and 46.7° is shown in Figure 3.9. The optimum design is $\alpha_1 = 46.7^{\circ}$ and $\alpha_2 = 43.3^{\circ}$. We will consider the case where the element is not rectangular in shape later in Section 3.6. As shown in the figure, the value of $|y|$ becomes maximum when $\theta = 90^{\circ}$. We need to pay more attention to the fact that when $\theta = 90^{\circ}$, the value of $|y|$ becomes very large in all cases. This large mismatch will cause problems for deployment, which will be discussed in detail in Section 3.7.

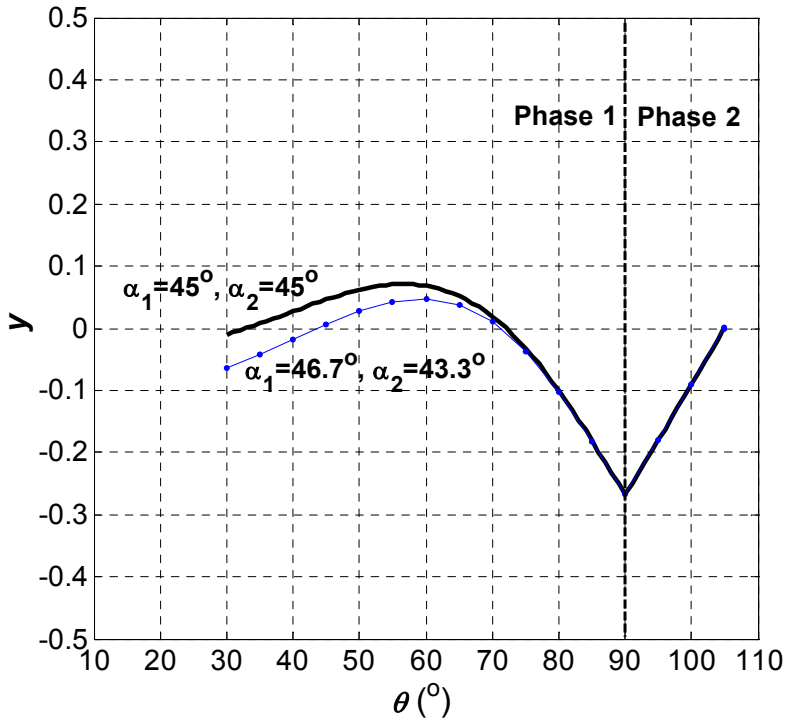

Figure 3.9 y vs. θ for the rectangle elements with α_1 = 45° and 46.7° when m = 6.

3.4 Length during deployment

As mentioned in Section 3.1, the length of the foldable cylindrical tube increases during expansion and decreases during folding. Once the elements are connected longitudinally, the other important geometric property of the stent graft, the total length of the foldable cylindrical tube, is calculated.

The total length L of the tube with the rectangle elements is defined in Figure 3.10. It is assumed that all elements behave exactly the same during deployment and the mismatch between each rows is not taken into account. During the first phase of deployment, i.e., $\theta_0 \le \theta \le 90^{\circ}$, L is given by

$$L = n \times AD - (n-1) \times O'Q \tag{3.39}$$

where AD has been calculated in Equation (3.20) and

$$O'Q = BQ\cos\varphi \tag{3.40}$$

in which φ has been calculated in Equation (3.23) and

$$BQ = l\cos\theta \tag{3.41}$$

Substitution of Equation (3.41) into Equation (3.40) gives

$$O'Q = \frac{l\sin 2\alpha_1 \cos^2\theta}{1-\sin^2\alpha_1 \sin^2\theta} \tag{3.42}$$

Hence

$$L = n\frac{2l}{\tan\alpha_1} - (n-1)\frac{l\sin 2\alpha_1 \cos^2\theta}{1-\sin^2\alpha_1 \sin^2\theta} \tag{3.43}$$

On the second phase of deployment, i.e., θ varies from 90^o to θ_1, L is given by

$$L = n\frac{2l}{\tan\alpha_1} \tag{3.44}$$

Results of the length calculations with various α_1, m and n during deployment will be given in Section 3.7.

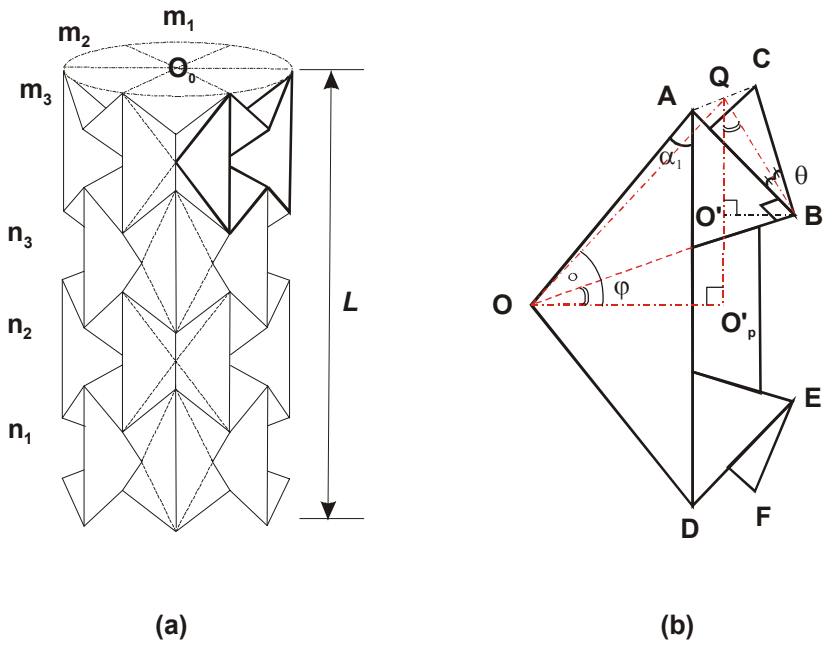

Figure 3.10 (a) Perspective view of the foldable cylindrical tube with rectangle elements and (b) one element during deployment.

3.5 Deformation during deployment

In Section 3.3 it has been found that the foldable cylindrical tube deforms during deployment because of the mismatch between the tube elements connected in the longitudinal direction. In this section the geometric parameter of the shortening of the fold during deployment is calculated to understand the deployment process. The results are useful in the determination the optimum design for the stent graft.

In Section 3.4 (Figure 3.7), it has been explained that in the top element, before it is connected to the lower element, the radii of nodes E_2 and F_2 are R_{o1} and R_{o2}, respectively. For the lower element, assuming that it behaves exactly the same as the top element during deployment, the radii of nodes A_1 and B_1 before it is connected to the element above are R_{o2} and R_{o1}, respectively. After connecting these two elements, the mismatch occurs. Assume that the radii R_{E2A1} and R_{F2B1} of the nodes E_2 or $A_1$and F_2 or B_1 are $(R_{o1} + R_{o2})/2$. In the cylindrical coordinate system, the coordinates of nodes E_2 or A_1 are (R_{E2A1}, δ_{E2A1}, Z_{E2A1}) and those of nodes F_2 or B_1 are (R_{F2B1}, δ_{F2B1}, Z_{F2B1}) where $\delta_{E2A1} = 0$; $\delta_{F2B1} = 180^o / m$, in which m is the number of the elements in the circumferential direction. If we denote the length between the nodes E_2 or $A_1$and F_2 or B_1 as l_a, we have

$$l_a = \left[\left(R_{E2A1}\cos\delta_{E2A1} - R_{F2B1}\cos\delta_{F2B1}\right)^2 + \left(R_{E2A1}\sin\delta_{E2A1} - R_{F2B1}\sin\delta_{F2B1}\right)^2 + \left(Z_{E2A1} - Z_{F2B1}\right)^2\right]^{\frac{1}{2}}$$

$$= \left[\left(\frac{R_{o1}+R_{o2}}{2} - \frac{R_{o1}+R_{o2}}{2}\cos\left(\frac{180^o}{m}\right)\right)^2 + \left(\frac{R_{o1}+R_{o2}}{2}\sin\left(\frac{180^o}{m}\right)\right)^2 + \left(Z_{E2A1} - Z_{F2B1}\right)^2\right]^{\frac{1}{2}} \quad (3.45)$$

R_{o1} has been calculated in Equations (3.25) and (3.28), and R_{o2} has been calculated in Equations (3.15) and (3.29). It is assumed that the difference between Z_{E2A1} and Z_{F2B1} is equal to the length $O'Q$. $O'Q$ was initially calculated using

Equation (3.42) when the mismatch was not taken into account. Now because the length between nodes E_2 or A_1 and nodes F_2 or B_1 is l_a, we need to modify Equation (3.42) where l_a replaces l. Hence

$$Z_{E2A1} - Z_{F2B1} = O'Q = \frac{l_a \sin 2\alpha_1 \cos^2 \theta}{1 - \sin^2 \alpha_1 \sin^2 \theta} \tag{3.46}$$

Considering Equations (3.46) and (3.45), we have

$$l_a = \left\{ \frac{\left(1 - \sin^2 \alpha_1 \sin^2 \theta\right)^2}{\left(1 - \sin^2 \alpha_1 \sin^2 \theta\right)^2 - \left(\sin 2\alpha_1 \cos^2 \theta\right)^2} \times \frac{\left(R_{o1} + R_{o2}\right)^2}{2} \left[1 - \cos\left(\frac{180^o}{m} \right) \right] \right\}^{\frac{1}{2}} \tag{3.47}$$

Results of the deformation of the fold with various α_1 and m during deployment are given in Section 3.7.

3.6 Generalisation of the basic element and its geometric properties

Only a rectangular element has been considered so far. The value of $\alpha_1 + \alpha_2$ is always 90^o. However, the element does not necessarily have to be rectangular. In this section an alternative design of the element will be explored.

A more general element is shown in Figure 3.11(a) where node B' replaces B. B' can be below or above B. The geometric parameters, such as radii, length and deformation of the cylindrical tube can be calculated accordingly.

Similar to the basic element in Section 3.3, R_{o1}, R_{o2} and R_i are defined as

$$R_{o1} = O_0 B' \tag{3.48}$$

$$R_{o2} = O_0 A \tag{3.49}$$

and

$$R_i = O_0 O \tag{3.50}$$

see Figure 3.11(b).

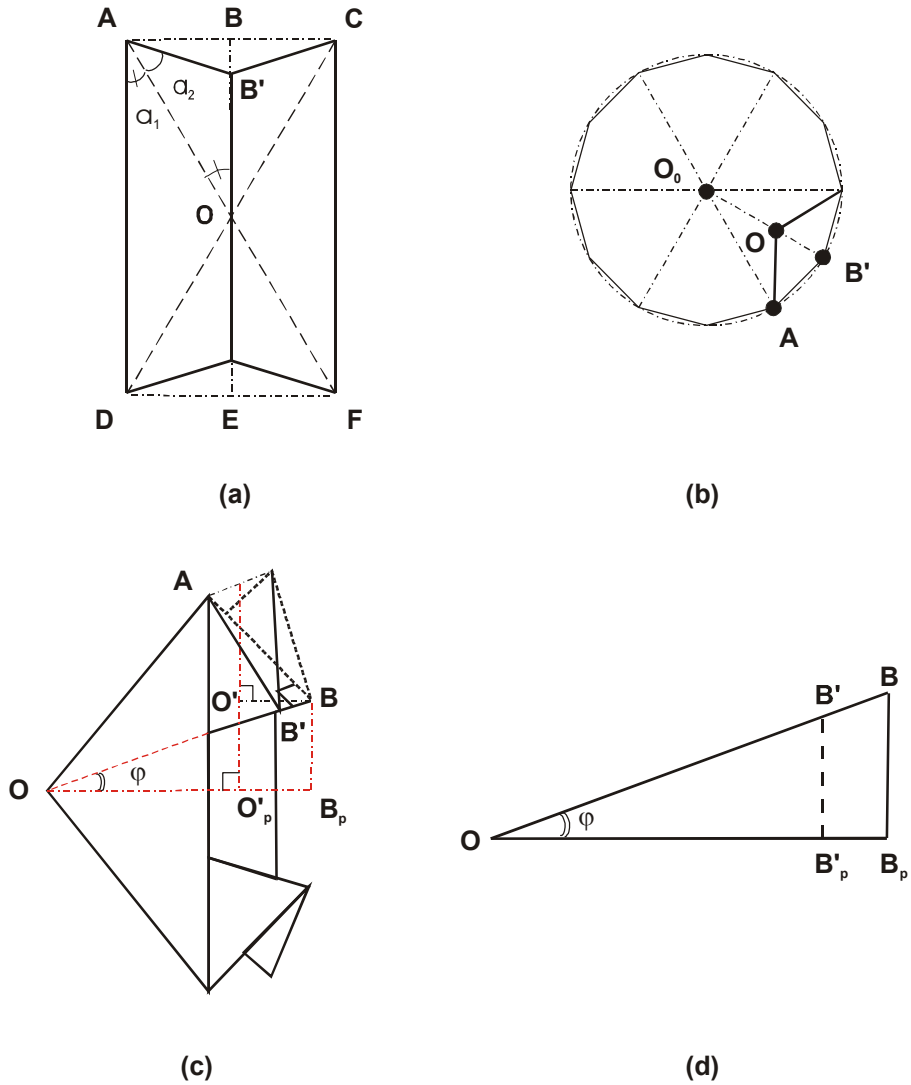

Figure 3.11 (a) A generalised element; (b) cross section views of the tube; (c) perspective view of the element and (d) geometric details.

From Figure 3.11(c) and (d),

$$R_{o1} = O_0O + OB'_p = R_i + OB_p \frac{OB'}{OB} \tag{3.51}$$

R_{o2} remains the same as it is in Equations (3.15) and (3.29) and R_i can also be found from Equations (3.27) and (3.30). Geometrically,

$$\frac{OB_p}{OB} = \cos\varphi \tag{3.52}$$

$$OB' = OB - BB' \tag{3.53}$$

where

$$\cos\varphi = \frac{\sin 2\alpha_1 \cos\theta}{1 - \sin^2\alpha_1 \sin^2\theta} \tag{3.54}$$

$$OB = \frac{l}{\tan\alpha_1} \text{ and } BB' = \frac{l}{\tan(\alpha_1 + \alpha_2)} \tag{3.55}$$

in which φ has been calculated in Equation (3.23). Substituting Equations (3.54) and (3.55) into (3.52) and (3.53) gives,

$$\frac{OB_p}{OB} = \frac{\sin 2\alpha_1 \cos\theta}{1 - \sin^2\alpha_1 \sin^2\theta} \tag{3.56}$$

$$OB' = \frac{l}{\tan\alpha_1} - \frac{l}{\tan(\alpha_1 + \alpha_2)} \tag{3.57}$$

Therefore, substituting Equations (3.27) and (3.30) and Equations (3.56) and (3.57) into (3.51) gives,

$$R_{o1} = \frac{l\sin\theta}{\tan\delta} - l\cos\theta + \left[\frac{l}{\tan\alpha_1} - \frac{l}{\tan(\alpha_1+\alpha_2)}\right] \times \left(\frac{\sin 2\alpha_1 \cos\theta}{1-\sin^2\alpha_1 \sin^2\theta}\right) \tag{3.58}$$

The relationships between y, which is the value of the mismatch between R_{o1} and R_{o2} normalised by l, and the deployment angle θ can also be considered. The results for various α_2 when $m = 6$ and $\alpha_1 = 45^o, 30^o$ or 60^o are drawn in Figure 3.12.

Figure 3.12(a) shows the value of y against θ when $\alpha_1 = 45^o$. When node B' is above node B, $\alpha_2 > 45^o$ and y is greater than zero. When node B' is below node B, $\alpha_2 < 45^o$ and y is smaller than zero. When $\alpha_1 = \alpha_2 = 45^o$, B' and B are at the same location, y is closer to zero. Therefore, it is preferable that α_2 is around 45^o to reduce mismatch between R_{o1} and R_{o2} during deployment. From Equation (3.38), the optimum design is when α_2 becomes 42.7^o. Figure 3.12(b) shows the value of y against θ when $\alpha_1 = 30^o$. y becomes closer to zero as α_2 decreases until 35.5^o. Figure 3.12(c) shows y against θ when $\alpha_1 = 60^o$. The optimum design is when α_2 becomes 44.2^o. However, it is found that the value of y varies dramatically during deployment, and $|y|$ is generally much larger than zero in comparison with the results when $\alpha_1 = 45^o$ or $\alpha_1 = 30^o$.

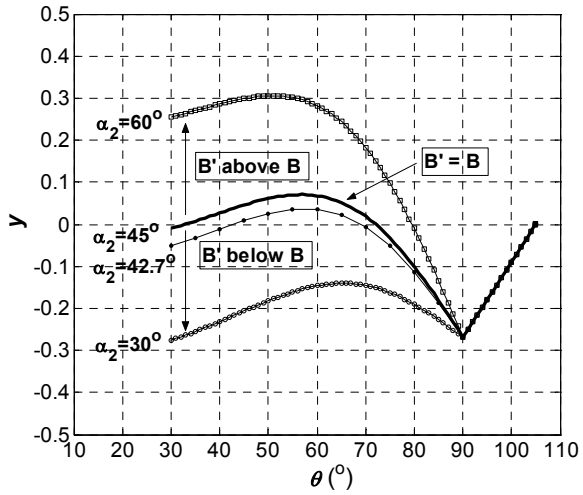

(a)

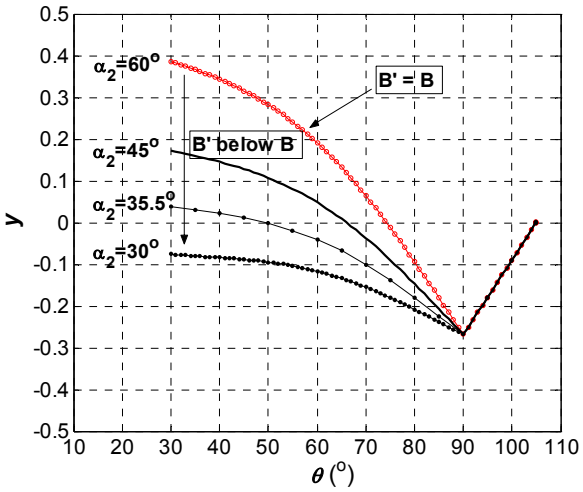

(b)

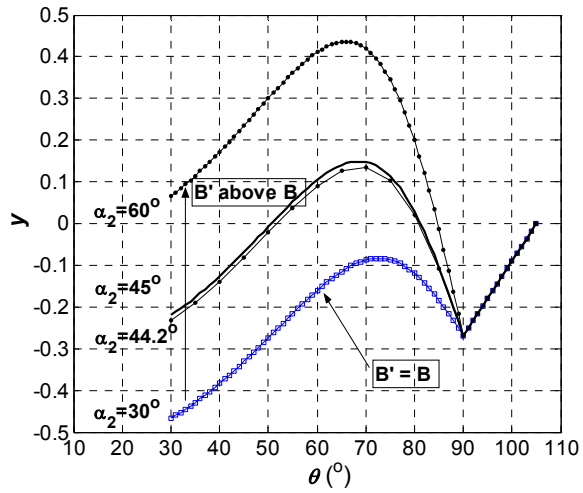

(c)

Figure 3.12 y **vs.** θ **for various** α_2 **when** m **= 6 and (a)** $\alpha_1 = 45^\circ$**, (b)** $\alpha_1 = 30^\circ$ **and (b)** $\alpha_1 = 60^\circ$**.**

Now consider the total length of the foldable cylindrical tube consisting of the general elements. Figures 3.13(a) and (b) show the perspective view of a single element during deployment and its planar projection, respectively. Since node B' replaces B, $O'Q$ in Equation (3.39) will also be replaced by $O'_2 Q$. Therefore, during the first phase of deployment, i.e., $\theta_0 \le \theta \le 90^o$, L is given by

$$L = n \times AD - (n-1) \times O'_2 Q \tag{3.59}$$

where

$$O'_2 Q = O'Q + HB' \tag{3.60}$$

in which AD and $O'Q$ has been calculated in Equations (3.20) and (3.42).

$$HB' = BB' \sin\varphi \tag{3.61}$$

where

$$BB' = \frac{l}{\tan(\alpha_1 + \alpha_2)} \tag{3.62}$$

$$\sin\varphi = \frac{\cos^2\alpha_1 - \sin^2\alpha_1 \cos^2\theta}{1 - \sin^2\theta \sin^2\alpha_1} \tag{3.63}$$

in which l is the length AB.

Substituting Equations (3.62) and (3.63) into (3.61) gives

$$HB' = \frac{l}{\tan(\alpha_1 + \alpha_2)} \frac{\cos^2\alpha_1 - \sin^2\alpha_1 \cos^2\theta}{1 - \sin^2\theta \sin^2\alpha_1} \tag{3.64}$$

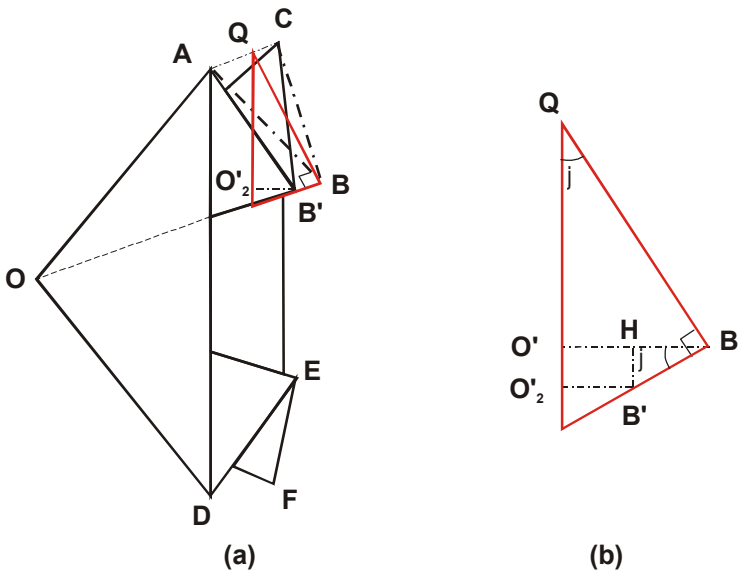

Figure 3.13 Most general element during deployment.
(a) Perspective view and (b) planar projection.

Then, substituting Equations (3.42) and (3.62) into (3.60) gives

$$O'_2 Q = \frac{l}{1-\sin^2\theta\sin^2\alpha_1}\left(\sin 2\alpha_1\cos^2\theta + \frac{\cos^2\alpha_1 - \sin^2\alpha_1\cos^2\theta}{\tan(\alpha_1+\alpha_2)}\right) \tag{3.65}$$

Consequently, L is defined as follow

$$L = n\frac{2l}{\tan\alpha_1} - \frac{(n-1)l}{1-\sin^2\theta\sin^2\alpha_1}\left(\sin 2\alpha_1\cos^2\theta + \frac{\cos^2\alpha_1 - \sin^2\alpha_1\cos^2\theta}{\tan(\alpha_1+\alpha_2)}\right) \tag{3.66}$$

On the second phase of deployment, i.e., θ varies from 90^o to θ_1, L is given by

$$L = nAD - (n-1)BB'$$

$$= n\frac{2l}{\tan\alpha_1} - \frac{(n-1)l}{\tan(\alpha_1+\alpha_2)} \tag{3.67}$$

The length l_a of the fold during deployment can also be calculated using Equation (3.45) in which the difference between Z_{E2A1} and Z_{F2B1} is equal to length $O'_2 Q$. $O'_2 Q$ has been calculated using Equation (3.65) and l needs to be replaced to $l_a \sin(\alpha_1 + \alpha_2)$ in order to take into account the mismatch between the elements. Therefore,

$$Z_{E2A1} - Z_{F2B1} = O'_2 Q = \frac{l_a \sin(\alpha_1 + \alpha_2)}{1 - \sin^2\theta \sin^2\alpha_1}\left(\sin 2\alpha_1 \cos^2\theta + \frac{\cos^2\alpha_1 - \sin^2\alpha_1 \cos^2\theta}{\tan(\alpha_1 + \alpha_2)}\right) \quad (3.68)$$

Considering Equations (3.68) and (3.45), we have

$$l_a = \left\{ \begin{array}{l} \dfrac{\left(1 - \sin^2\alpha_1 \sin^2\theta\right)^2}{\left(1 - \sin^2\alpha_1 \sin^2\theta\right)^2 - \sin^2(\alpha_1 + \alpha_2)\left(\sin 2\alpha_1 \cos^2\theta + \dfrac{\cos^2\alpha_1 - \sin^2\alpha_1 \cos^2\theta}{\tan(\alpha_1 + \alpha_2)}\right)^2} \\ \times \dfrac{(R_{o1} + R_{o2})^2}{2}\left[1 - \cos\left(\dfrac{180^o}{m}\right)\right] \end{array} \right\}^{\frac{1}{2}} \quad (3.69)$$

3.7 Models and discussions

In this section, results of radius, length and deformation of the foldable cylindrical tube during deployment will be presented. Although the optimum designs are $\alpha_1 = 46.7^o$ and $\alpha_2 = 43.3^o$, $\alpha_1 = 45^o$ and $\alpha_2 = 42.7^o$, or $\alpha_1 = 30^o$ and $\alpha_2 = 35.5^o$, the values of each α_1 and α_2 are close enough so that two special cases are considered where $\alpha_1 = \alpha_2 = 45^o$ and $\alpha_1 = \alpha_2 = 30^o$. For convenience, the model with $\alpha_1 = \alpha_2 = 45^o$ and $\alpha_1 = \alpha_2 = 30^o$ are called as Models 1 and 2, respectively. Model 1 uses the rectangular elements and Model 2 uses the general elements. Models 1 and 2 when $m = 6$ in the fully folded and expanded configurations are shown in Figure 3.14.

(a)

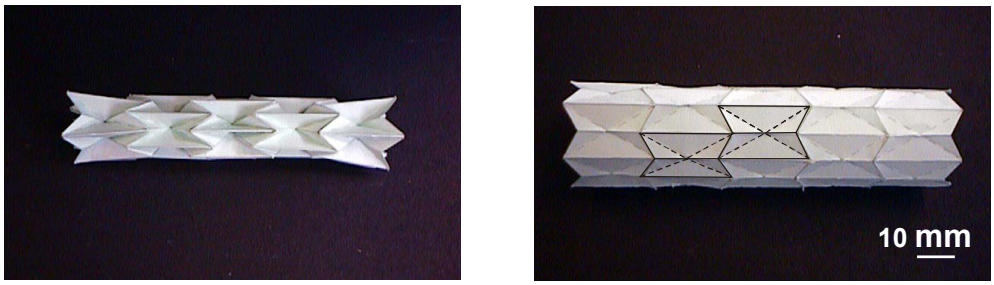

(b)

Figure 3.14 (a) Models 1 and (b) Model 2
in its fully folded and fully expanded configurations when *m* = 6.

3.7.1 Radius

Figures 3.15(a) and (b) show the outer and inner radii of each model, R_{o1}, R_{o2} and R_i of Models 1 and 2 normalized by the length l during deployment when m is 6. θ_0 and θ_1, which are deployment angles in the fully folded and expanded configurations, are 30^o and 105^o, respectively. The inner radius R_i gradually increases during deployment for both models. For Model 1, R_{o1} is greater than R_{o2} from θ being between 33^o and 72^o. For Model 2, R_{o1} is always smaller than R_{o2}. The ratio of the value of R_{o1} in the fully folded configuration to R_{o1} in the fully expanded configuration is denoted as R^*. R^* is 51.4% and 47.8% for Models 1 and 2, respectively.

Figure 3.16 shows the relationship of the ratio R^* vs. m. It is noted that R^* decreases with respect to an increasing m in both models. In other words, a larger m

enables the models to be folded more compactly in the radial direction. In comparison with Model 1, Model 2 has a lower value of R^* and hence folds more compactly until m is 9. However, the difference in the values of R^* between Models 1 and 2 becomes insignificant when m is larger than 9.

As mentioned in Chapter 2, the fully folded radius of the currently available stent grafts for the treatment of oesophageal cancer and abdominal aortic aneurysm is about 20 - 35% of the fully expanded radius. When m = 9, R^* of Models 1 and 2 is 34.7% and 33%, respectively. When m = 20, R^* becomes about 15.7% for both models. Table 3.2 shows dimensions of the origami stent graft with various values for m when the expanded diameter is 26 mm. A greater m results in more compact folding. However, it causes difficulty in folding process since each element becomes small and potentially the thickness of the stent graft material becomes an important issue. Therefore, m of the element should be selected to balance these two factors.

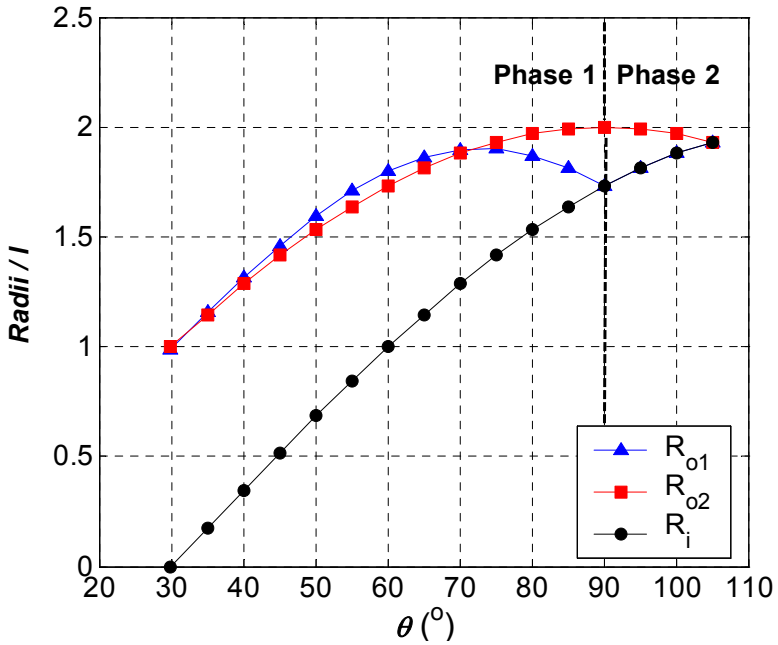

(a)

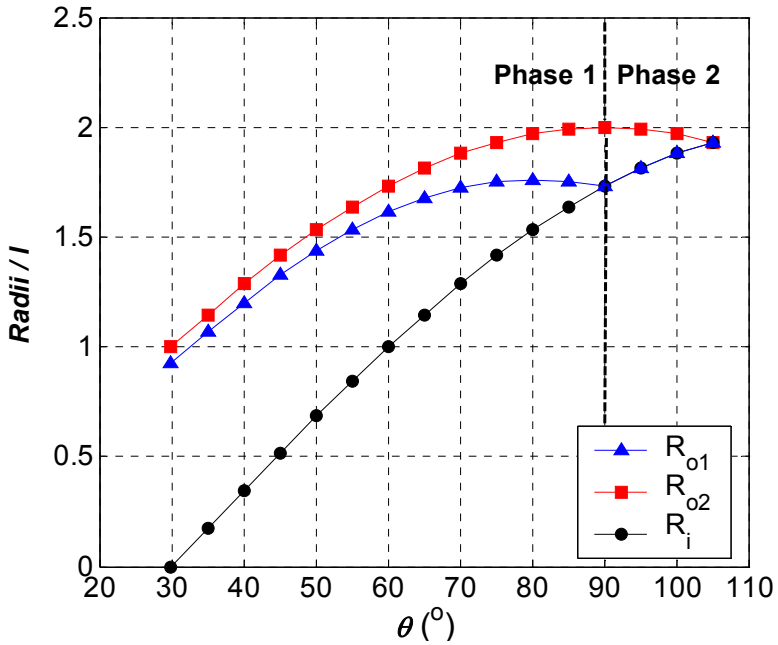

(b)

Figure 3.15 R_{o1}, R_{o2} **and** R_i **vs.** θ **when** m **= 6. (a) Model1 and (b) Model 2.**

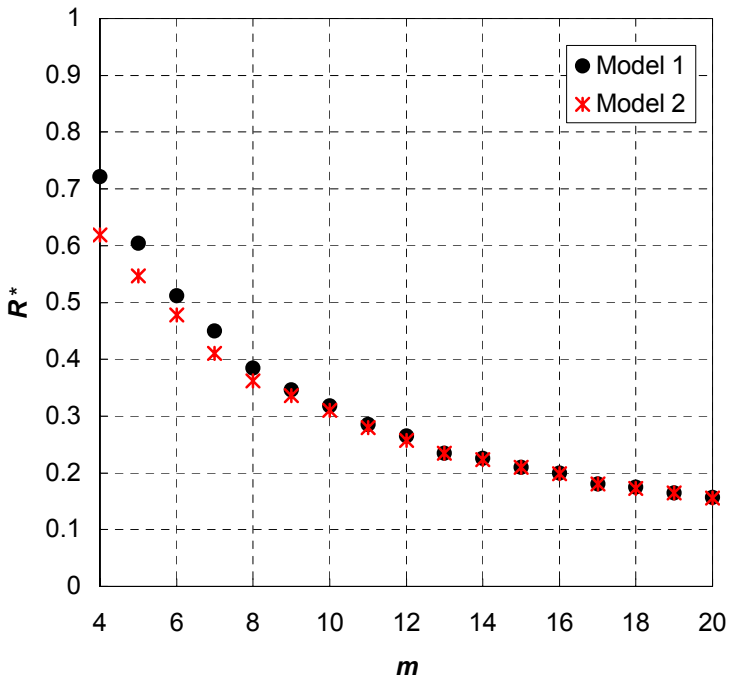

Figure 3.16 ***R**** **vs.** ***m*.**

Table 3.2 Dimensions of the origami stent graft with various *m*.

Expanded diameter (mm)	26				
m	9	12	14	16	20
R^* x 100 (%)	34.7	26.5	22.5	20.0	15.7
Folded diameter (mm)	9.00	6.89	5.85	5.2	4.08
Catheter (Fr./mm)	28/9.24	21/6.93	18/5.94	16/5.28	13/4.29
Element size (mm)	9.08	6.80	5.83	5.11	4.08

3.7.2 Length

The ratio of the total length L in the fully folded configuration with respect to in the fully expanded configuration is denoted as L^*. Figure 3.17 shows L^* versus various n for $m = 6$. It is noted that for both models, the ratio L^* slowly decreases as n increases. Both models are folded more compactly in the longitudinal direction as n increases. The value of L^* becomes nearly constant when n is greater than 8, so there is no particular benefit in increasing the number n of the elements above 8. In Model 1, it can be folded up into 63% of the length in its fully expanded configuration, while, in the Model 2, it is 86%. Compared to Model 1, Model 2 is folded less compactly in the longitudinal direction. Therefore, Model 1 is preferred for uses where longitudinal folding is desirable to allow access of the stent graft to a narrow blocked site, whereas Model 2 is preferred for uses when medical practitioners prefer the longitudinal shortening to be minimised.

Figure 3.18 shows the value of L^* of Model 1 for different values of m when $n = 8$. It is noted that L^* becomes smaller as m increases. This is because the deployable angle in the fully folded configuration, θ_0, becomes smaller as m increases. Thus a larger m reduces L^* and R^*.

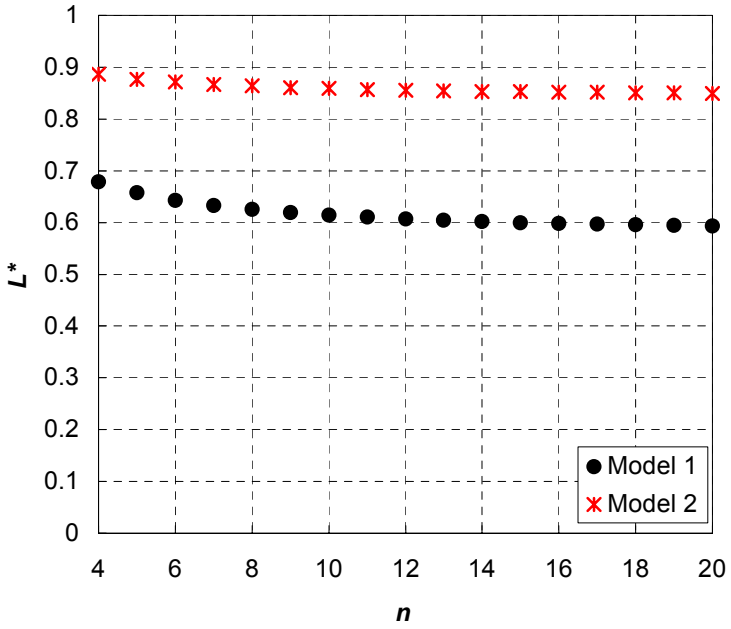

Figure 3.17 *L vs. *n* when *m* = 6.**

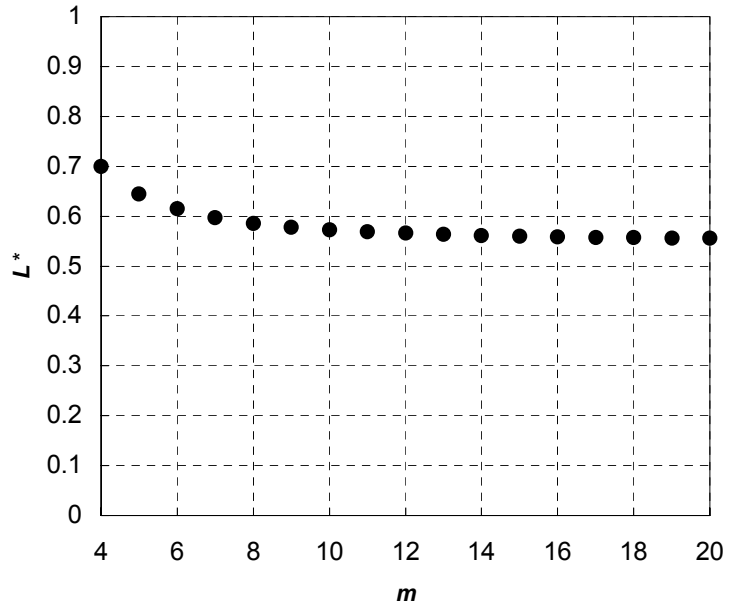

Figure 3.18 *L vs. *m* when *n* = 8.**

3.7.3 Deformation

Figure 3.19 shows a plot of l_a / l_o versus the deployable angle θ, for various element numbers m for Model 1. l_o is the original length between nodes A_1 and B_1 before connecting two elements in a longitudinal direction. Consider the initial case where $m = 6$. From the figure, it is noted that l_a / l_o becomes 1 when $\theta = 33^o$ and 72^o. This is where the foldable cylindrical tube admits unstrained configuration. Between these angles the shortening of l_a is less than 0.3%. However it increases dramatically while θ approaches 90^o. When θ becomes 105^o where the tube is fully expanded, l_a becomes equal to l_o again and the structure becomes unstrained. Moving from one unstrained configuration to the other between θ of 72^o to 105^o requires larger deformation. The structure may not be expanded smoothly, and could even be snapped. The behaviour of the shortening is different when m increases, which is shown next.

If we take m = 18, l_a is not shortened very much when θ is around 90^o. The deformation between unstrained configurations at the end of deployment, i.e. when $\theta = 85^o$ and 92.5^o, is smaller. However, it can be seen that it is shortened more at the beginning of deployment compared with the case m = 6. The optimum solution is m = 9. The shortening of l_a is less than 1.5 % during the deployment.

Figure 3.20 shows a plot of l_a / l_o versus the deployment angle θ for various element number m for Model 2. The value of l_a / l_o becomes smaller as m increases. For m = 18, the shortening of l_a is less than 0.4%, which is less than the results for Model 1.

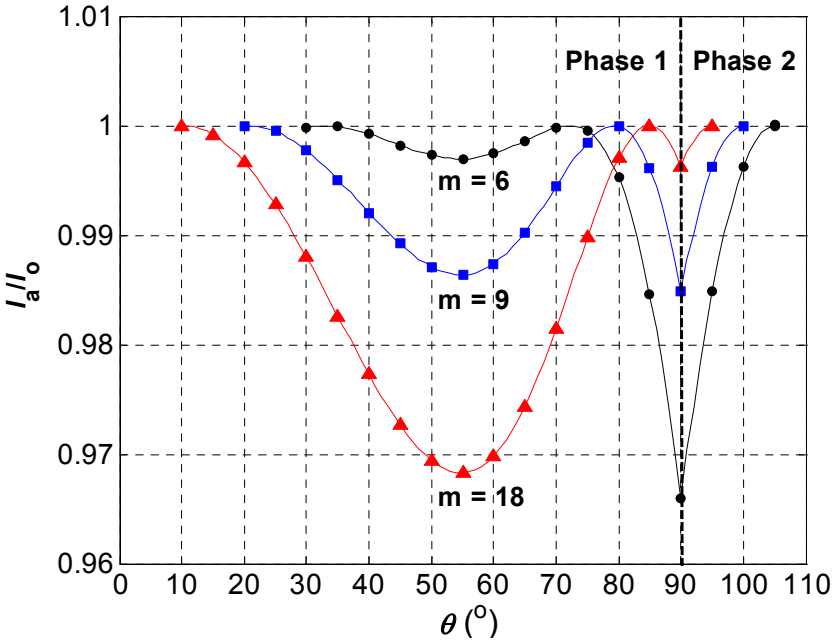

Figure 3.19 Plots of I_a/I_o vs. θ with various m for Model 1.

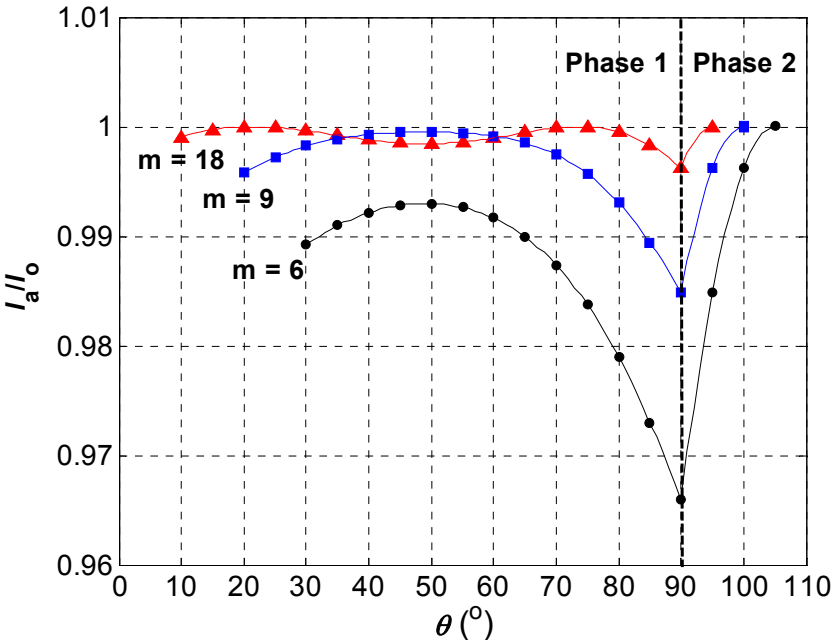

Figure 3.20 Plots of I_a/I_o vs. θ with various m for Model 2.

3.8 Variation of the folding patterns

In addition to folding patterns using the general elements, further variations are possible.

3.8.1 Centre folding

The pattern of folds described in the previous sections can be generalised further by the introduction of an extra valley fold between the intersections O and P (see Figure 3.21). Node B' can be below or above node B. The length OP affects the overall length when the structure is fully folded but has no effect on the radius during folding.

3.8.2 Double folding

The pattern of folds described so far involves a peak at the centre of an element when it is folded (see Figure 3.23a). As shown in Figure 3.22 additional folding lines can be added in the centre in order to level the peak. The element can be folded more compactly and therefore the overall radius can be further reduced (see models shown in Figure 3.23b).

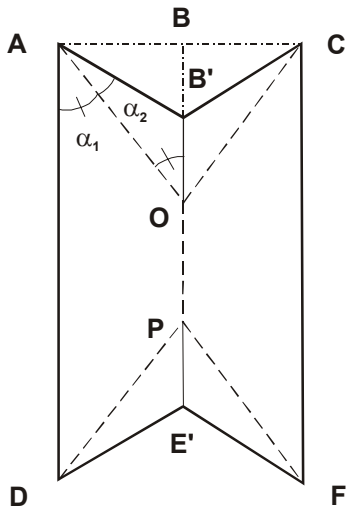

Figure 3.21 Element with an extra central valley between O and P.

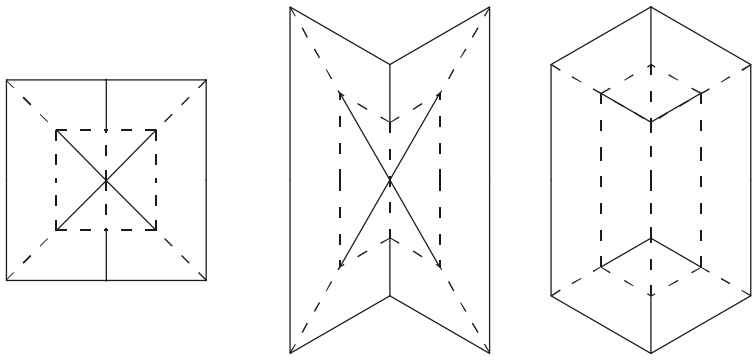

Figure 3.22 Elements with additional folds in the centre.

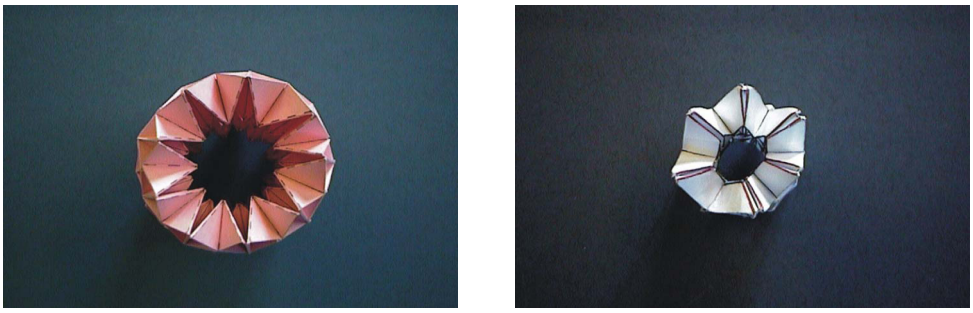

(a) **(b)**

Figure 3.23 The end views of the foldable tubes
(a) with and (b) without peaks at the centre.

3.8.3 Unsymmetrical folding

The patterns of folds discussed so far are symmetrical about both the central longitudinal fold and an imaginary circumferential line. However, this is not essential.

For example, Figures 3.24(a) shows diagrams of the elements which are symmetrical only about the central longitudinal fold. The upper and lower halves of the element are based on the rectangle element and the general element, respectively. The development of the foldable cylindrical tube with the elements is shown in Figure 3.24(b). The neighbouring rows are shifted by a half-unit. Accordingly, the

element of alternate rows is reversed in the longitudinal direction as illustrated in bold outline.

The diagram of the other possible element design is shown in Figures 3.25, which are symmetrical only about an imaginary line in circumferential direction. It is a combination of two halves of different elements, except that the central longitudinal fold extends at an angle to the longitudinal direction.

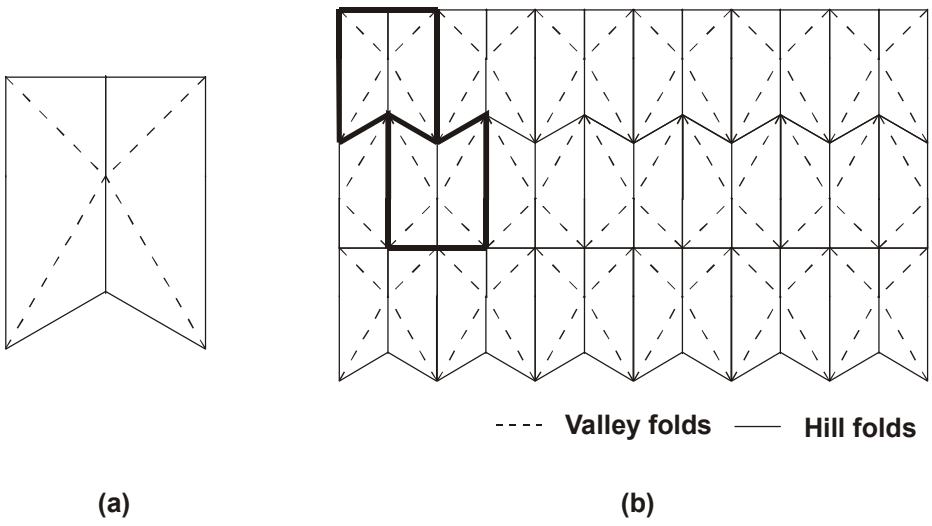

Figure 3.24 (a) Single element with a folding pattern and (b) the development of the foldable cylindrical tube with the unsymmetrical folding.

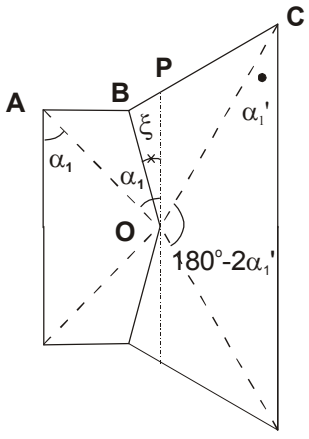

Figure 3.25 Element with the unsymmetrical folding.

As shown in Figure 3.25, the fold OB leans to angle ξ with respect to OP. Since the sum of alternation of the centre angles of node O is equal to 180^o to make an element foldable, see Equation (2.5)

$$2(\alpha_1 - \xi) + 180^o - 2\alpha_1' = 180^o \tag{3.70}$$

Consequently,

$$\xi = \alpha_1 - \alpha_1' \tag{3.71}$$

Unlike the previous models, this foldable cylindrical tube cannot be divided into such elements by simple repetition. A possible arrangement using the element is shown in Figure 3.26.

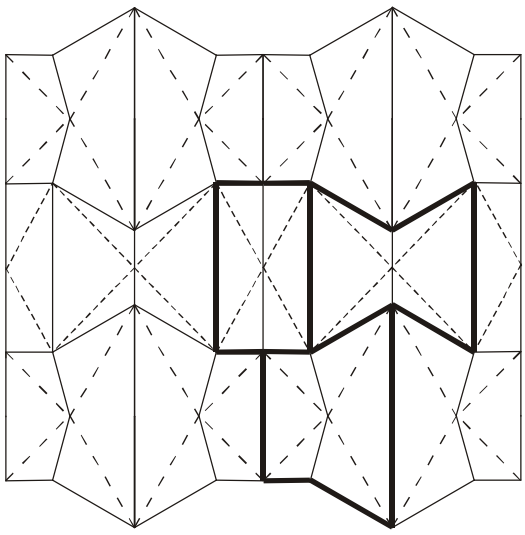

Figure 3.26 Pattern of a foldable cylindrical tube using three types of elements.

3.8.4 Folding pattern for conical tubes

The patterns of folds discussed previously are applicable to cylindrical tubes. They can be modified for conical tubes. Figure 3.27 shows the development of the foldable conical tube. The photographs of a cone in its fully folded and expanded configurations are shown in Figure 3.28.

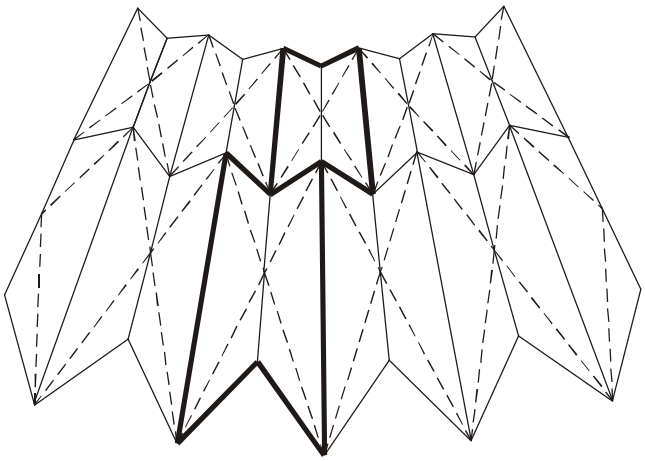

Figure 3.27 Elements for a foldable conical tube.

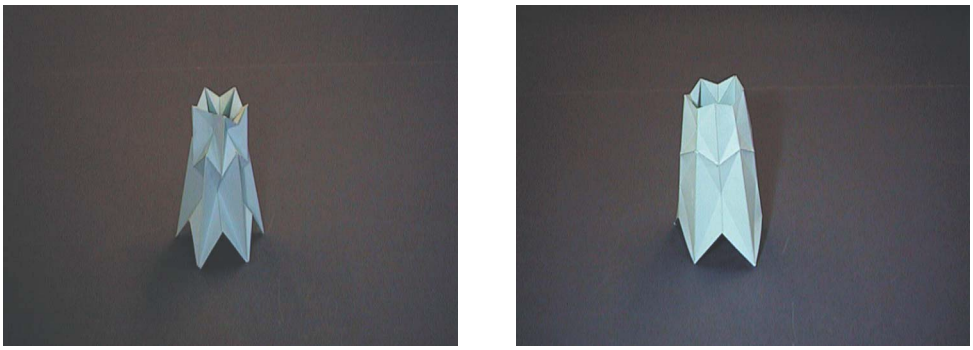

(a) **(b)**

Figure 3.28 Foldable cone in its (a) fully folded and (b) fully deployed configurations.

3.9 Conclusions

In this chapter a new type of a single piece stent graft has been developed. A detailed symmetric design of a foldable cylindrical tube for the stent graft has been presented. Folding is achieved by dividing the structure into a series of identical foldable elements. Particular attention has been paid to two types of elements: rectangular elements and general elements. Folding patterns for each type of element was obtained. Both patterns allow the stent graft to be folded and expanded both radially and longitudinally. The important geometric parameters of the elements and of the foldable cylindrical tube are defined and analysed.

The relationships among the design of the elements, the number of elements in the circumferential and longitudinal directions and the folded dimensions of the stent graft have been derived. It has been found that compact folding in the radial direction can be achieved by increasing the number of circumferential elements. However, a large number of elements may cause manufacturing difficulty. A compromise can be found to address both concerns. It has also been found that the stent graft can be folded compactly in the longitudinal direction as both the number of the circumferential and longitudinal elements increase, and that the ratio of its constriction depends on the design of the element.

A geometric mismatch during deployment has also been identified. The elements have to deform when the structure is expanded. Optimum designs which minimise the deformation have been found.

Variations to the general folding patterns of both cylindrical and conical tubes have also been discussed, though without detailed geometric calculation.